Available online at www.sciencedirect.com
ScienceDirect
Journal of Non-Crystalline Solids 352 (2006) 5578–5585
JOURNAL OF NON-CRYSTALLINE SOLIDS
www.elsevier.com/locate/jnoncrysol

Thermodynamic model for solid-state amorphization of pure elements by mechanical-milling

Y.H. Zhao *

Materials Physics and Applications Division, Los Alamos National Laboratory, Los Alamos, NM 87545, United States

Received 6 April 2006; received in revised form 1 September 2006

Abstract

Mechanical-milling induced solid-state amorphization (SSA) has been observed in some covalent metalloids (Si, Ge, Se), but never in pure metals at room temperature. In this paper, a thermodynamic model was proposed for the SSA of the pure elements. In the model, a large Gibbs free energy of a grain boundary, compared with the free energy of a crystalline–amorphous interface, provides driving force for the amorphization. The critical grain size required for the SSA, therefore, can be determined from the condition when the Gibbs free energy of the nanocrystalline state is equal to that of amorphous state. The predicted critical grain sizes for SSA generally agree with the experimentally observed values for nonmetallic elements, but are much smaller than the minimum grain sizes of the metallic elements obtained by long-time mechanical-milling.
© 2006 Elsevier B.V. All rights reserved.

PACS: 64.60.Cn; 64.70.Nd; 81.20.Ev

Keywords: Mechanical alloying; Glass transition; Phases and equilibria

1. Introduction

Solid-state amorphization (SSA) from crystalline parent phases has been intensively studied in the past few decades (for reviews, see [1–3]). Techniques inducing SSA include irradiation- and hydrogen-assisted amorphization, interdiffusion of metallic multi-layers, pressure-induced vitrification, mechanically-driven amorphization, etc. Theoretical explanations for SSA can be divided into atomistic lattice instability and thermodynamically-driven. Atomistic models of the various SSA processes have one common feature that they lead to static disordering of the parent crystalline phase by incorporation of non-equilibrium defects. Due to the incorporated atomic disorder, the crystalline phase is driven into an instability at which the crystalline phase collapses into an amorphous phase. Several lattice instability models have been proposed for SSA. They include vibrational [4], elastic [5], topological [6], entropical [7] and Lindeman melting criterion [8]. From a thermodynamic aspect, elemental mixing or accumulation of lattice imperfections (point defects, dislocations, grain boundaries (GBs), chemical disorder, etc.) raises the Gibbs free energy of the crystalline phase above that of the amorphous phase, and when this occurs, SSA is possible [9–11].

Mechanically-driven SSA has been observed in many binary alloy systems by mechanical alloying (MA) of the corresponding elemental crystalline powder mixtures or by mechanical-milling (MM) of the inter-metallic compounds [2,3,12]. In the former case, negative heat of mixing and fast diffusion of one of the elements favor the formation of amorphous alloy phases. In the latter case, the MM induces not only accumulation of lattice defects but also chemical disordering in the lattice, leading to SSA. While most studies of mechanically-driven SSA have focused on binary alloy systems, there are also a few reports on amorphization of pure elements. Some covalent metalloids (C, Si, Ge and Se) are amorphized by a variety

* Tel.: +1 505 665 6774; fax: +1 505 667 2264.
E-mail address: zhao@lanl.gov

0022-3093/$ - see front matter © 2006 Elsevier B.V. All rights reserved.
doi:10.1016/j.jnoncrysol.2006.09.021

Table 1
Experimentally observed critical grain sizes, $D^*_{obs.}$, and lattice expansions, Δa^*, at the onset of the amorphization in Si [16,17], Ge [19] and Se [22] by mechanical-milling process

Elements	Si	Ge	Se
$D^*_{obs.}$ (nm)	3	2.5–3.5	13
Δa^* (%)	0.2	0.2–0.4	0.2

of methods including ion-implantation [13], vapor deposition [14], indentation [15] and ball-milling. Upon MM, partial and/or full amorphization have been observed in Si [16–18], Ge [19] and Se [20–22]. The MM-induced SSA of the metalloids were found to occur when the critical grain sizes and the critical lattice expansions were reached, as summarized in Table 1. In contrast to metalloids, the amorphization of pure metals has never been realized by MM at room temperature. Instead, the MM process produced nanocrystalline microstructures with minimum grain sizes for all pure metals (for reviews, see Refs. [23,24]).

In this paper, a thermodynamic model was proposed for the MM-induced SSA of pure elemental systems. According to this model, the critical grain sizes for SSA of different metals and nonmetals were calculated and compared with the experimental values.

2. Thermodynamic model

Based on the experimental observations [16–22], the mechanical-milling process mainly introduces the GBs (or grain-size-refinement), lattice expansion and the microstrain, etc. lattice imperfections into the initially crystalline lattice, which increase the Gibbs free energy of the ball-milled polycrystalline powders. When the Gibbs free energy of the milled nanocrystalline system is enhanced to be larger than that of the amorphous state, a driving force for the amorphization, from the Gibbs free energy difference between the two states, then exists.

Assuming that a spherical nanocrystallite with a diameter of D was transformed into the amorphous phase within a nanocrystalline sample, as schematically represented in Fig. 1, the Gibbs free energy change $\Delta G(T)$ will be:

$$\Delta G(T) = \frac{4\pi}{3}\left(\frac{D}{2}\right)^3(\Delta G_v - \Delta E_1 + \Delta E_2) + 4\pi\left(\frac{D}{2}\right)^2(\gamma_{ca} - \gamma_{gb}), \quad (1)$$

where ΔG_v is the Gibbs free energy difference per unit volume between the amorphous and crystalline states. Assuming that super-cooled liquid and amorphous phases are identical and neglecting the heat capacity (c_p) difference between the crystalline and amorphous states, ΔG_v can be approximated by [25]:

$$\Delta G_v(T) = \frac{\Delta H_m(T_m - T)}{T_m}, \quad (2)$$

where ΔH_m represents the fusion enthalpy change and T_m the melting temperature with the index denoting "melting". ΔE_1 represents the elastic energy density change (per unit volume) due to the lattice expansion (resulted from vacancies) and the microstrain (caused by dislocations), $\langle\varepsilon^2\rangle^{1/2}$, induced by ball-milling:

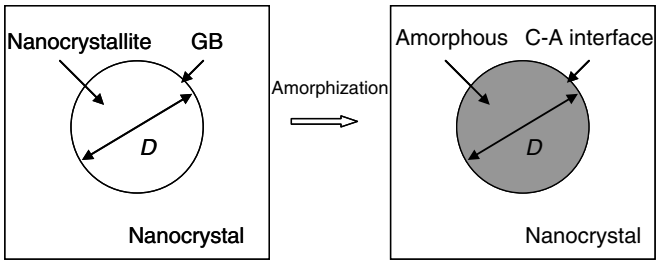

Fig. 1. Schematic representation of a spherical nanocrystallite with a diameter of D transformed into amorphous state within a nanocrystalline sample. The grain boundary (GB) was transformed into a crystalline–amorphous (C–A) interface after amorphization.

$$\Delta E_1 = \left[\frac{V_{nc} - V_c}{V_c}\right]^2 K + (\langle\varepsilon^2\rangle^{1/2})^2 K, \quad (3)$$

where V_{nc} and V_c are the molar volumes of nanocrystalline and crystalline phases, respectively, K is the bulk modulus for the nanocrystalline solid. ΔE_2 denotes the change in strain energy density (per unit volume) resulting from the volume change upon the amorphization. According to Allen et al. [26]:

$$\Delta E_2 = \frac{18\mu K\varepsilon'^2 f}{4\mu + 3K}, \quad (4)$$

where μ is the shear modulus of the nanocrystalline solid, and f is a factor to account for the effect of a free surface on the strain energy density, which is taken to be 1.0 in the present case. ε' is the hydrostatic strain associated with the fractional volume change during amorphization, $\varepsilon' = \frac{1}{3}(V_a - V_{nc})/V_{nc}$, where V_a is the molar volume of amorphous state. γ_{ca} and γ_{gb} are, respectively, the crystalline–amorphous (C–A) interfacial energy and the GB energy of the nanocrystalline phase. In the present case, γ_{ca} is assumed to be temperature independent, and γ_{gb} is temperature dependent. At the right side of Eq. (1), $(4\pi/3)(D/2)^3[\Delta G_v - \Delta E_1 + \Delta E_2]$ is a bulk term, and $4\pi(D/2)^2(\gamma_{ca} - \gamma_{gb})$ is an area term.

When $\Delta G(T) = 0$ and $\partial\Delta G(T)/\partial D = 0$, the critical grain sizes $D_1^*(T)$ and $D_2^*(T)$ can be calculated by:

$$D_1^*(T) = \frac{3}{2}D_2^*(T) = \frac{6(\gamma_{gb} - \gamma_{ca})}{\Delta G_v - \Delta E_1 + \Delta E_2}. \quad (5)$$

$D_1^*(T)$ is the critical grain size where the SSA onset occurs at temperature T, and $D_2^*(T)$ is the critical grain size where the driving force for the SSA (or amorphization transformation velocity) is the largest.

3. Calculation results

3.1. $\Delta G(293)$ and $D_1^*(293)$ of Si, Ge and Se

Using available data of ΔH_m, T_m, V_{nc}, V_c, $\langle\varepsilon^2\rangle^{1/2}$, K, μ, V_a, γ_{ca} and γ_{gb} for a certain element, the Gibbs free energy

change, $\Delta G(293)$, at room temperature ($T = 293$ K) as a function of the mean grain size, D, can be obtained based on Eqs. (1)–(4).

From Ref. [27], ΔH_m of the elemental Se is 6.694 kJ/mol (e.g., 0.407×10^9 J/m^3 with density of 4.80 g/cm^3 and molar mass of 78.96 g/mol) and T_m is 494 K. $\Delta G_v(293)$ is therefore calculated as 165.6×10^6 J/m^3 for the elemental Se. Similarly, $\Delta G_v(293)$ are calculated as 3464.5 and 2051.9 J/m^3 for Si and Ge, respectively.

From Ref. [28], the Young's modulus and Poisson's ratio of crystalline Se are 58 GPa and 0.447, respectively. Therefore, the bulk modulus and the shear modulus of crystalline Se can be calculated as $K = 182.39$ GPa and $\mu = 20.04$ GPa. Here the modulus of nanocrystalline phase is assumed to be equal to that of coarse-grained (CG) polycrystalline phase. The volume expansion, $(V_{nc} - V_c)/V_c$, and the microstrain, $\langle \varepsilon^2 \rangle^{1/2}$, at the onset of the MM-induced SSA of nanocrystalline Se were 0.30% and 0.39%, respectively [22]. ΔE_1 was then calculated as 4.42×10^6 J/m^3 for nanocrystalline Se. Similarly, ΔE_1 for nanocrystalline Si and Ge can be calculated as 8.48 and 10.65×10^6 J/m^3 with the lattice expansions of 0.2% and 0.4%, respectively. Therefore, ΔE_1 are much smaller than $\Delta G_v(293)$ values.

ε' in Eq. (4) can be written as:

$$\varepsilon' = \frac{1/\rho_a - 1/\rho_{nc}}{3(1/\rho_{nc})}, \tag{6}$$

because both nanocrystalline and amorphous phases have the same molar mass. Here ρ_{nc} and ρ_a are the densities of the nanocrystalline and amorphous phases at room temperature. The density of amorphous phase, $\rho_a(T)$, has the following relationship with temperature T:

$$\rho_a(T) = \rho_a^0 + (T - T_m) d\rho_a/dT, \tag{7}$$

where ρ_a^0 is the density of amorphous phase at melting point T_m, and $d\rho_a/dT$ is temperature coefficient of the density of amorphous phase. For nanocrystalline Se, assuming $\rho_{nc} = \rho_c$, where ρ_c is the density of the CG Se at room temperature, then $\rho_{nc} = 4.80$ g/cm^3 [27]. With the assumption that the super-cooling liquid Se and amorphous Se are identical, ρ_a^0 is 3.989×10^6 g/m^3, and $d\rho_a/dT = -1.44 \times 10^3$ g/Km^3 [29] for amorphous Se. Therefore, ρ_a of amorphous Se can be calculated as 4.278×10^6 g/m^3 at room temperature. So, ε' is 0.041 for Se, and $\Delta E_2 = 173.2 \times 10^6$ J/m^3 at room temperature, which is comparable with $\Delta G_v(293)$ value. Similarly, ΔE_2 for Si and Ge are calculated to be 967.7 and 245.9 J/m^3, respectively.

The grain boundary free energy of nanocrystalline Se prepared by crystallization from amorphous Se solid has been found to be varied against the mean grain size [30]. With decreasing grain size from 23 to 8 nm, γ_{gb} of Se decreased from 0.33 to 0.25 J/m^2. Here $\gamma_{gb} = 0.25$ J/m^2 was taken for nanocrystalline Se. γ_{gb} are not available experimentally for nanocrystalline Si and Ge, even not for CG polycrystalline Si and Ge. From simulation, the average energies of high-angle GBs for crystalline Si and Ge are found to be 1.46 [31] and 1.12 J/m^2 [32], respectively. Here it is assumed that the GB energy of nanocrystalline phase is equal to that of CG polycrystalline counterpart, as verified by Ref. [33]. The crystalline–amorphous interfacial energies, γ_{ca}, for Se, Si and Ge are equal to 0.021 [34], 0.167 and 0.176 J/m^2 [35], respectively.

Table 2 lists the calculated values of the different terms ($\Delta G_v(293)$, ΔE_1, ΔE_2, γ_{gb}, γ_{ca}) at the right side of Eq. (1) for the elemental Se, Si and Ge at room temperature. Fig. 2 shows the variations of $\Delta G(293)$, bulk term $((4\pi/3)(D/2)^3[\Delta G_v(293) - \Delta E_1 + \Delta E_2])$ and area term $(4\pi(D/2)^2(\gamma_{ca} - \gamma_{gb}))$ against the mean grain size D for the elemental Se at room temperature.

With refining D to 0, the bulk term decreases from positive (unfavorable to amorphization) to zero; while the area term increases from negative (favorable to amorphization) to 0. As a results, the Gibbs free energy change, $\Delta G(293)$, which is the combination of the bulk and area terms, decreases from positive to zero at $D_1^*(293)$ (=4.1 nm for Se), then reaches a minimum value $\Delta G^*(293)$ ($= -1.766 \times 10^{-18}$ J) at $D_2^*(293)$ (=2.7 nm), finally trends to 0 with the further refinement of D to 0. In other words, when D was refined to the critical grain size $D_1^*(293)$, the Gibbs free energy of the milled nanocrystalline system is enhanced to be equal to that of amorphous state, suggesting a thermodynamic phase equilibria between the amorphous and nanocrystalline states, or an onset of SSA; when D was further refined to $D_2^*(293)$, the driving force for SSA reaches the largest value $\Delta G^*(293)$.

The calculated $D_1^*(293)$ for Si and Ge are 1.8 and 2.5 nm, respectively, as listed in Table 2. These values are in agreement with the experimentally observed critical grain sizes, $D_{obs.}^*$, of SSA, as listed in Table 1. For the SSA of nanocrystalline Se, $D_1^*(293)$ (=4.1 nm) is smaller than $D_{obs.}^*$ (13 nm). This is because the XRD peak-broadening method calculates the average grain size of the ball-milled powders, and some existed large-sized grains will enhance $D_{obs.}^*$ above the actual grain size of SSA (e.g., $D_1^*(293)$).

Table 2
Lists of the Gibbs free energy differences per unit volume between the amorphous and crystalline states, $\Delta G_v(293)$, the elastic energy density changes, ΔE_1, the strain energy density changes, ΔE_2, the grain boundary energies, γ_{gb} [30–32], the crystalline–amorphous interfacial energies, γ_{ca} [34,35], and the calculated critical grain sizes, $D_1^*(293)$, for SSA of the metalloid Se, Si and Ge at room temperature

Elements	$\Delta G_v(293)$ (10^6 J/m^3)	ΔE_1 (10^6 J/m^3)	ΔE_2 (10^6 J/m^3)	γ_{gb} (J/m^2)	γ_{ca} (J/m^2)	$D_1^*(293)$ (nm)
Se	165.6	4.42	173.2	0.25 [30]	0.021 [34]	4.1
Si	3464.5	8.48	967.7	1.46 [31]	0.167 [35]	1.8
Ge	2051.9	10.65	245.9	1.12 [32]	0.176 [35]	2.5

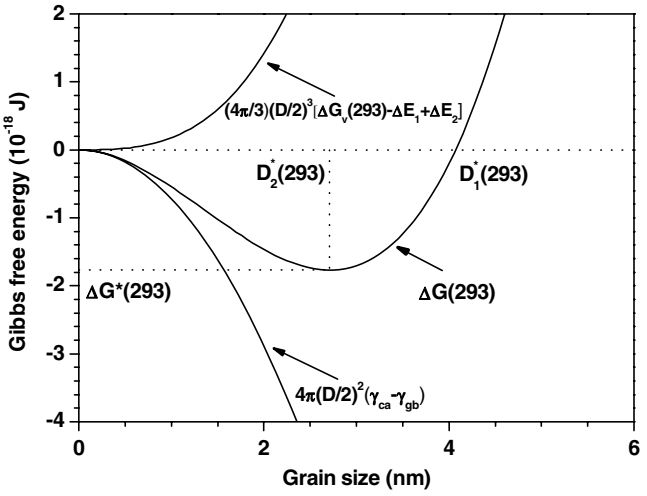

Fig. 2. The Gibbs free energy change after solid-state amorphization, $\Delta G(293)$, and the bulk $((4\pi/3)(D/2)^3[\Delta G_v(293) - \Delta E_1 + \Delta E_2])$ and area $(4\pi(D/2)^2(\gamma_{ca} - \gamma_{gb}))$ terms against the mean grain size D for the elemental Se at room temperature. $D_1^*(293)$ (=4.1 nm) is the critical value for the onset of SSA transformation and $D_2^*(293)$ (=2.7 nm) is the critical value where the driving force for SSA reaches the largest ($\Delta G^*(293) = -1.766 \times 10^{-18}$ J).

3.2. $\Delta G(293)$ and $D_1^*(293)$ of metallic elements

Similarly, the metallic critical grain sizes for the onset of SSA at room temperature, $D_1^*(293)$, can be calculated by using the literature values.

During the calculation, $\Delta G_v(293)$ for different metals are calculated by using the values from Ref. [27]. ΔE_1 was ignored since it is much smaller than $\Delta G_v(293)$ and ΔE_2. To calculate ΔE_2 value, the shear modulus and bulk modulus are taken from Ref. [28], and the ε' values for different metals are calculated using the literature values from Ref. [29].

The grain boundary energy of metals can be obtained from different measurements [36] including precise calorimetry, zero creep [37,38], phase-boundary intersection and calculation from dislocation theory, etc. The zero creep measurement is the most well-tried method for different metallic elements. In this method, the GB energy at the temperature T close to melting point, γ_{gb}^T, is calculated from the measured solid surface energy, γ_s^T, and the dihedral angles of GB groove formed by thermal etching at the surface by:

$$\gamma_{gb}^T = n\gamma_s^T, \tag{8}$$

where n can be calculated from the dihedral angles of GB groove. Both γ_{gb}^T and γ_s^T are temperature dependent, and the temperature coefficient of γ_s^T, $d\gamma_s^T/dT$, can be experimentally measured or calculated. Therefore, the GB energy at room temperature, γ_{gb}^{RT}, can be obtained from the values of n, γ_s^T and $d\gamma_s^T/dT$ assuming n is temperature independent by:

$$\begin{aligned} \gamma_s^{RT} &= \gamma_s^T + (293 - T)d\gamma_s^T/dT \\ \gamma_{gb}^{RT} &= n\gamma_s^{RT} \end{aligned}, \tag{9}$$

where γ_s^{RT} is solid surface energy at room temperature.

For elemental Ag, Al, Au, Cu, Fe, Ni and Pt, Ref. [39] summarizes the values of γ_{gb}^T, $d\gamma_{gb}^T/dT$ (calculated from n and $d\gamma_s^T/dT$). So, γ_{gb}^{RT} for these metals can be calculated by:

$$\gamma_{gb}^{RT} = \gamma_{gb}^T + (293 - T)d\gamma_{gb}^T/dT. \tag{10}$$

Table 3 lists the values of γ_{gb}^T, T, $d\gamma_{gb}^T/dT$ and γ_{gb}^{RT} for elemental Al, etc.

For the other metals, $d\gamma_s^T/dT$ are not available from the zero creep measurement. Ref. [40] gives the calculated values for $d\gamma_s^T/dT$, and Ref. [41] lists the recommended values for solid surface energy at 0 K, γ_s^0. The n values for Co, Cr, Mo, Nb, Sn, Ta, and W can be obtained from the zero creep measurements [42–46]. The n values were taken as 1/3 for Cd, Hf, Ir, Pd, Rh, Ru, Ti, Zr and Zn, which can not be found in literature. Therefore, γ_s^{RT} and γ_{gb}^{RT} for these metals can be calculated according to Eq. (9). Table 4 lists the values of γ_s^0, $d\gamma_s^T/dT$, γ_s^{RT}, n and γ_{gb}^{RT} for elemental Cd, etc. The γ_{ca} values of different metals were taken from Ref. [47].

Table 5 lists the calculated values of $\Delta G_v(293)$, ΔE_2, γ_{gb}^{RT}, γ_{ca} and $D_1^*(293)$ for above metals. The experimentally observed minimum grain sizes during MM process, $D_{obs.}^*$, for different metals [48–56] are also listed in Table 5.

From Table 5, $D_1^*(293)$ of the most metals are in the range of 1–2 nm, except that $D_1^*(293)$ of Ag (2.0 nm), Cd (3.6 nm), Sn (2.8 nm), Zr (2.1 nm) and Zn (2.5 nm) are larger than 2 nm. Compared with $D_{obs.}^*$, $D_1^*(293)$ is about one order of magnitude smaller. This explains the reason that the SSA of metals is difficult to occur at room temperature, because ball-milling process can not refine the grain size to the critical grain size required by SSA.

3.3. Temperature dependence of $D_1^*(T)$ of metals

The calculated critical grain size for SSA, $D_1^*(T)$, from the thermodynamic model is temperature dependent,

Table 3
Values of grain boundary energies at temperature T, γ_{gb}^T, temperature coefficients of grain boundary energy, $d\gamma_{gb}^T/dT$, and calculated grain boundary energies at room temperature ($T = 293$ K) and at 0 K, γ_{gb}^{RT} and γ_{gb}^0, for elemental Ag, Al, Au, Cu, Fe, Ni and Pt [39]

Elements	Ag	Al	Au	Cu	Fe	Ni	Pt
γ_{gb}^T (J/m^2)	0.375	0.324	0.378	0.625	0.468	0.866	0.660
T (K)	1223	723	1273	1198	1723	2333	1573
$d\gamma_{gb}^T/dT$ (10^{-3}J/m^{2}K)	−0.10	−0.12	−0.10	−0.10	−0.25	−0.20	−0.18
γ_{gb}^{RT} (J/m^2)	0.468	0.376	0.476	0.716	0.826	1.074	0.890
γ_{gb}^0 (J/m^2)	0.497	0.411	0.505	0.745	0.899	1.333	0.943

Table 4
Values of solid surface energies at 0 K, γ_s^0 [41], temperature coefficients of solid surface energy, $d\gamma_s^T/dT$ [40], solid surface energies at room temperature, γ_s^{RT}, ratios of grain boundary energy to solid surface energy, n [42–46], the grain boundary energies at room temperature and at 0 K, γ_{gb}^{RT} and γ_{gb}^0, for the metallic Cd, Co, Cr, Hf, Ir, Mo, Nb, Pd, Rh, Ru, Sn, Ta, Ti, W, Zr and Zn

Elements	γ_s^0 (J/m^2) [41]	$-d\gamma_s^T/dT$ (10^{-2}J/m^{2}K) [40]	γ_s^{RT} (J/m^2)	n	γ_{gb}^{RT} (J/m^2)	γ_{gb}^0 (J/m^2)
Cd	0.740	0.014	0.699	1/3	0.233	0.247
Co	2.550	0.020	2.491	0.39 [42]	0.972	0.995
Cr	2.300	0.017	2.250	0.4 [43]	0.900	0.920
Hf	2.150	0.011	2.118	1/3	0.706	0.717
Ir	3.000	0.016	2.953	1/3	0.984	1.000
Mo	3.000	0.014	2.959	0.30 [44]	0.888	0.900
Nb	2.700	0.014	2.659	0.36 [45]	0.957	0.972
Pd	2.050	0.016	2.003	1/3	0.668	0.683
Rh	2.700	0.016	2.653	1/3	0.884	0.900
Ru	3.050	0.017	3.000	1/3	1.000	1.017
Sn	0.675	0.011	0.643	0.24 [46]	0.154	0.162
Ta	3.150	0.014	3.109	0.28 [44]	0.858	0.882
Ti	2.100	0.013	2.062	1/3	0.687	0.700
W	3.675	0.015	3.631	0.37 [43]	1.344	1.360
Zr	2.000	0.011	1.968	1/3	0.656	0.667
Zn	0.990	0.018	0.937	1/3	0.312	0.330

The n values are estimated as 1/3 when they are not available from the literature.

Table 5
Lists of Gibbs free energy differences per unit volume between crystalline and amorphous states, $\Delta G_v(293)$, strain energy density changes, ΔE_2, grain boundary energies at room temperature, γ_{gb}^{RT}, crystalline–amorphous interfacial energies, γ_{ca} [47], calculated critical grain sizes, $D_1^*(293)$ at room temperature, and experimentally observed minimum grain sizes by mechanical-milling, $D_{obs.}^*$, [48–56] for different metallic elements

Elements	$\Delta G_v(293)$ (10^6 J/m^3)	ΔE_2 (10^6 J/m^3)	γ_{gb}^{RT} (J/m^2)	γ_{ca} (J/m^2) [47]	$D_1^*(293)$ (nm)	$D_{obs.}^*$(nm)
Ag	838.8	12.6	0.468	0.184	2.0	22 [48]
Al	740.8	33.4	0.376	0.154	1.7	22 [49]
Au	960.4	5.6	0.476	0.200	1.7	–
Cd	241.5	11.1	0.233	0.081	3.6	–
Co	2039.8	40.4	0.972	0.345	1.8	14 [50]
Cr	2015.5	108.3	0.900	0.381	1.5	9 [50]
Cu	1442.9	3.2	0.716	0.263	1.9	11 [51]
Fe	1627.7	115.8	0.826	0.326	1.7	8 [52]
Hf	1558.9	119.6	0.706	0.322	1.4	13 [50]
Ir	2725.5	293.6	0.984	0.466	1.0	6 [49]
Mo	3057.2	86.7	0.888	0.490	0.8	5 [53]
Nb	2169.7	59.8	0.957	0.399	1.5	9 [50]
Ni	2199.1	156.8	1.074	0.356	1.8	12 [49]
Pd	1666.3	3.8	0.668	0.302	1.3	7 [49]
Pt	1841.9	388.8	0.890	0.334	1.5	–
Rh	2251.2	163.4	0.884	0.384	1.2	7 [49]
Ru	2560.6	15.1	1.000	0.443	1.3	13 [50]
Sn	181.5	4.9	0.154	0.066	2.8	–
Ta	2640.6	26.4	0.858	0.477	0.9	6 [54]
Ti	1232.6	414.2	0.687	0.271	1.5	27 [55]
W	3420.3	71.6	1.344	0.590	1.3	9 [50]
Zr	1036.6	107.4	0.656	0.242	2.1	13 [50]
Zn	461.4	4.9	0.312	0.119	2.5	20[a] [56]

[a] Milled at liquid-nitrogen temperature.

because the terms at the right side of Eq. (5) are varying against the temperature. To simplify the calculation process, the strain energy density, ΔE_2, and the C–A interfacial energy, γ_{ca}, are assumed to be temperature independent for metals, because both terms are much smaller than the Gibbs free energy difference, ΔG_v, and the GB energy, γ_{gb}, respectively.

Table 6 lists the values of $\Delta G_v(0)$ at 0 K for metals, which were calculated from Eq. (2). Comparing Table 6 with Table 5, the $\Delta G_v(0)$ is larger than the $\Delta G_v(293)$ for a certain metallic element. From Eqs. (8)–(10), the GB energies at 0 K, γ_{gb}^0, can be calculated, as listed in Tables 3 and 4. Therefore, the critical grain size for SSA at 0 K, $D_1^*(0)$, can be calculated, as listed in Table 6. Except

Table 6
Lists of Gibbs free energy differences per unit volume between crystalline and amorphous states at 0 K, $\Delta G_v(0)$, grain boundary energies at 0 K, γ^0_{gb}, and calculated critical grain sizes, $D^*_1(0)$, for different metallic elements

Elements	$\Delta G_v(0)$ (10^6 J/m^3)	γ^0_{gb} (J/m^2)	$D^*_1(0)$ (nm)
Ag	1099.9	0.497	1.7
Al	1079.7	0.411	1.4
Au	1229.7	0.505	1.5
Cd	476.5	0.247	2.0
Co	2445.0	0.995	1.6
Cr	2337.0	0.920	1.3
Cu	1840.1	0.745	1.6
Fe	1942.2	0.899	1.6
Hf	1765.8	0.717	1.3
Ir	3055.1	1.000	0.9
Mo	3402.1	0.900	0.7
Nb	2429.5	0.972	1.4
Ni	2648.8	1.333	2.1
Pd	1985.0	0.683	1.2
Pt	2150.0	0.943	1.4
Rh	2590.7	0.900	1.1
Ru	2897.0	1.017	1.2
Sn	432.3	0.162	1.3
Ta	2899.0	0.882	0.8
Ti	1451.5	0.700	1.4
W	3716.2	1.360	1.2
Zr	1202.4	0.667	1.9
Zn	799.6	0.330	1.6

elemental Ni, $D^*_1(0)$ is smaller than $D^*_1(293)$ for a certain metal.

Fig. 3 shows the calculated $D^*_1(T)$ against T for elemental Al. $D^*_1(T)$ decreases from 4.2 nm to 1.7 nm with decreasing T from 933 K (melting point of Al) to 293 K. When $T = 0$ K, $D^*_1(0) = 1.4$ nm. From literature, cryo-milling can effectively decrease the $D^*_{obs.}$ by reducing the dynamic recovery [23]. Nevertheless, the cryo-milling still can not refine the $D^*_{obs.}$ close to the predicted $D^*_1(T)$. To author's knowledge, there is no report that cryo-milling can realize the SSA of pure metals in literature.

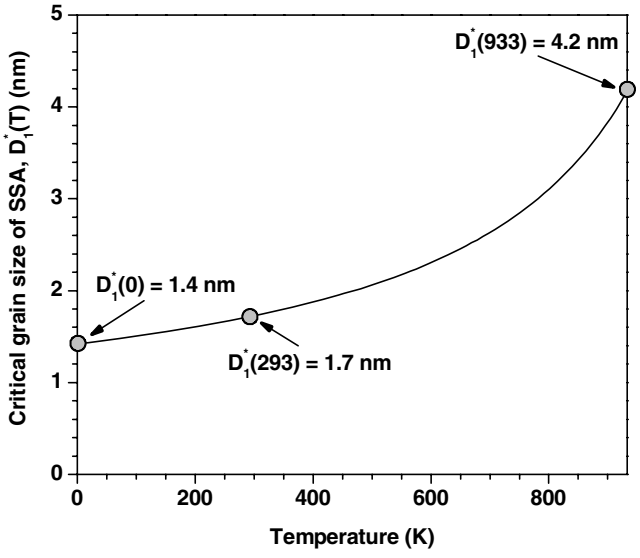

Fig. 3. The calculated critical grain size for the onset of SSA transformation, $D^*_1(T)$, against temperature T for elemental Al. $D^*_1(T)$ decreases with decreasing temperature.

4. Discussion

To compare the thermodynamic-model predicted critical grain sizes for SSA with the experimentally observed minimum grain sizes, Fig. 4 plots $D^*_1(293)$ versus $D^*_{obs.}$. The calculated $D^*_1(293)$ have large uncertainties, because the experimentally measured solid surface energies, grain boundary energies and n values, etc. have large error bars and the approximations were taken during calculations. However, from Fig. 4, the present thermodynamic calculation can give a good explanation for the different behaviors of metals and nonmetals during mechanical-milling process. For metals, all the data points (open squares) are located at the bottom-right corner of the figure, and the data points of nonmetals (open circles) are at the top-left corner. This means that for nonmetals, ball-milling can refine the grain size close to the required critical grain sizes for SSA (i.e., SSA is possible at room temperature), however, for metals, the minimum grain sizes realized by ball-milling are much larger than the critical grain sizes required by SSA (e.g., SSA is impossible at room temperature by ball-milling process).

Fig. 4 also shows that, except for the data point of Ti, $D^*_1(293)$ and $D^*_{obs.}$ have a good relationship: $D^*_{obs.}$ increases with an increase of $D^*_1(293)$, which means the larger critical grain size for SSA, the more difficult for grain-refinement (the larger minimum grain size) by ball-milling. The data scattering is caused by the large uncertainties of both

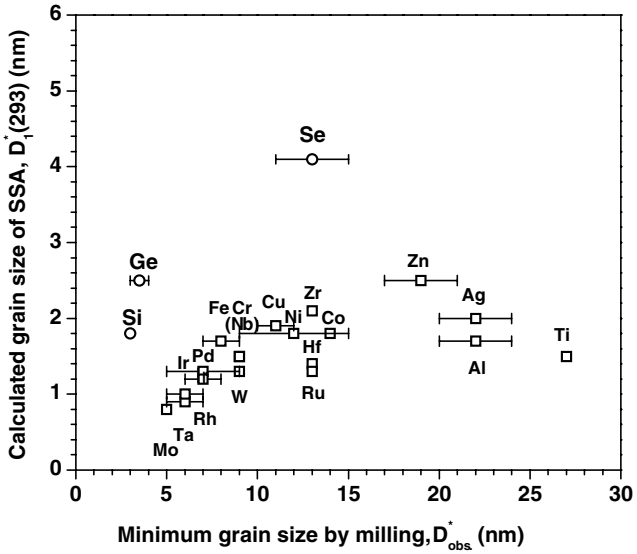

Fig. 4. Plot of the calculated critical grain sizes of amorphization at room temperature, $D^*_1(293)$, against the experimentally observed minimum grain sizes, $D^*_{obs.}$, during ball-milling process [17,19,22,48–56] for various elements (as indicated in the figure). The amorphized metalloids Si, Ge and Se (open circles) are at the top-left corner, and the non-amorphized metals (open squares) by mechanical-milling are at bottom-right corner.

$D_1^*(293)$ and $D_{obs.}^*$. It has been found that $D_{obs.}^*$ values are also related with the detailed experimental conditions: such as the milling energy and the ratio of ball-to-powder, etc. [23]. Therefore, $D_{obs.}^*$ from different groups may not be comparable. The calculated $D_1^*(293)$ of Ti is probably smaller, because the approximation of n as 1/3 may result in a small GB energy. The observed $D_{obs.}^*$ of Zn was obtained by mechanical-milling at liquid-nitrogen temperature, which is smaller than that milled at room temperature. The relationship of $D_1^*(293)$ and $D_{obs.}^*$ in Fig. 4 may give an alternative explanation for the observed different $D_{obs.}^*$ values of different metals by mechanical-milling, except for the dislocation recovery model [49,57–59]. This needs further investigation which is beyond the main aim and conclusion of the present paper.

From literature, the amorphous metals can be prepared by low-temperature evaporation or sputtering [60–62], because the low-temperature evaporation and sputtering processes are totally different from the grain-refinement by mechanical-milling. The formers form amorphous states from "bottom-up" (atomic accumulation), while the later from "top-down". The evaporated and sputtered atoms were assembled on substrates, cooled by liquid helium or nitrogen, with too low energy to crystallize. However, the amorphous metals prepared by low-temperature evaporation or sputtering are unstable and crystallize at temperatures below room temperature. The thermodynamic model proposed in the paper was based on grain-refinement mechanisms of SSA. Another possible mechanism is hydrostatic pressure. It was reported that Si and Ge in single crystal form became amorphous under the indentor of a hardness machine [15]. The pressures existing in ball-milling could be significant and may also be a possible source of the amorphization, which is beyond the main scope of this paper and needs further investigation.

5. Conclusion

In summary, a thermodynamic model was proposed for the crystal-to-amorphous phase transition of pure elemental systems induced by mechanical-milling process. The model predicts critical grain sizes required for the MM-induced SSA of the pure elements, which can be determined from the Gibbs free energy balance between the nanocrystalline and amorphous states. The predicted critical grain sizes for different elements agree generally with the experimental observations.

References

[1] W.L. Johnson, Prog. Mater. Sci. 30 (1986) 81.
[2] C.C. Koch, J.D. Whittenberger, Intermetallics 4 (1996) 339.
[3] C. Suryanarayana, Prog. Mater. Sci. 46 (2001) 1.
[4] H.J. Fecht, W.L. Johnson, Mater. Sci. Eng. A 133 (1991) 427.
[5] L.E. Rehn, P.R. Okamoto, J. Pearson, R. Bhadra, M. Grimsditch, Phys. Rev. Lett. 59 (1987) 2987.
[6] T. Egami, Y. Waseda, J. Non-Cryst. Solids 64 (1984) 113.
[7] H.J. Fecht, W.L. Johnson, Nature 334 (1988) 50.
[8] N.Q. Lam, P.R. Okamoto, MRS Bull. 19 (1994) 41.
[9] R.B. Schwarz, W.L. Johnson, Phys. Rev. Lett. 51 (1983) 415.
[10] D. Wolf, P.R. Okamoto, S. Yip, J.F. Lutsko, M. Kluge, J. Mater. Res. 5 (1990) 286.
[11] R. Benedictus, A. Böttger, E.J. Mittemeijer, Phys. Rev. B 54 (1996) 9109.
[12] A.W. Weeber, H. Bakker, Physica B 153 (1988) 93.
[13] E.P. Donovan, F. Spaepen, D. Turnbull, J.M. Poate, D.C. Jacobson, J. Appl. Phys. 57 (1985) 1795.
[14] S. Vepřek, Z. Iqbal, F.-A. Sarott, Philos. Mag. B 45 (1982) 137.
[15] D.R. Clarke, M.C. Kroll, P.D. Kirchner, R.F. Cook, B.J. Hockey, Phys. Rev. Lett. 60 (1988) 2156.
[16] E. Gaffet, M. Harmelin, J. Less-Common Met. 157 (1990) 201.
[17] T.D. Shen, C.C. Koch, T.L. Mccormick, R.J. Nemanich, J.Y. Huang, J.G. Huang, J. Mater. Res. 10 (1995) 139.
[18] J.Y. Huang, H. Yasuda, H. Mori, Philos. Mag. Lett. 79 (1999) 305.
[19] E. Gaffet, Mater. Sci. Eng. A 136 (1991) 161.
[20] T. Fukunaga, M. Utsumi, H. Akatsuka, M. Misawa, U. Mizutani, J. Non-Cryst. Solids 205–207 (1996) 531.
[21] G.J. Fan, F.Q. Guo, Z.Q. Hu, M.X. Quan, K. Lu, Phys. Rev. B 55 (1997) 11010.
[22] Y.H. Zhao, Z.H. Jin, K. Lu, Philos. Mag. Lett. 79 (1999) 747; Y.H. Zhao, Y.T. Zhu, T. Liu, J. Appl. Phys. 95 (2004) 7674.
[23] C.C. Koch, Nanostruct. Mater. 2 (1993) 109; C.C. Koch, Nanostruct. Mater. 9 (1997) 13.
[24] H.J. Fecht, in: G.C. Hadjipanayis, R.W. Siegel (Eds.), Nanophase Materials, Kluwer Academic Publisher, Netherland, 1994, p. 125; H.J. Fecht, Nanostruct. Mater. 6 (1995) 33.
[25] D. Turnbull, J. Appl. Phys. 21 (1950) 1022.
[26] G.L. Allen, W.W. Gile, W.A. Jesser, Acta Metall. 28 (1980) 1695.
[27] Periodic Table of the Elements, Sargent-Welch Scientific Company, Skokie, Illinois, 1979.
[28] E.A. Brandes, G.B. Brook, Smithells Metals Reference Book, 7th Ed., Butterworth-Heinemann Ltd., Oxford, 1992, p. 15–2.
[29] E.A. Brandes, G.B. Brook, Smithells Metals Reference Book, 7th Ed., Butterworth-Heinemann Ltd., Oxford, 1992, p. 14-7.
[30] K. Lu, N.X. Sun, Philos. Mag. Lett. 75 (1997) 389.
[31] S.R. Phillpot, D. Wolf, Philos. Mag. B 60 (1989) 545.
[32] M.C. Payne, P.D. Bristowe, J.D. Joannopoulos, Phys. Rev. Lett. 58 (1987) 1348.
[33] A. Tschöpe, R. Birringer, H. Gleiter, J. Appl. Phys. 71 (1992) 5391.
[34] K.F. Kelton, Solid State Phys. 45 (1991) 75.
[35] X.C. Zeng, D. Stroud, J. Phys.: Condens. Matter 1 (1989) 1779.
[36] M.C. Inman, E.R. Tipler, Metall. Rev. 8 (1963) 105.
[37] I. Sawai, M. Nishida, Z. Anorg. Allg. Chem. 190 (1930) 375.
[38] H. Udin, A.J. Shaler, J. Wulff, Trans. AIME 185 (1949) 186.
[39] L.E. Murr, Intrefacial Phenomena in Metals and Alloys, Addison-Wesley, Reading, MA, 1975, p. 131.
[40] A.R. Miedema, Z. Metallkd. 69 (1978) 287.
[41] F.R. de Boer, R. Boom, W.C.M. Mattens, A.R. Miedema, A.K. Niessen, Cohesion in Metals-Transition Metall Alloys, North-Holland, Amsterdam, 1988, p. 662.
[42] T.A. Roth, Mater. Sci. Eng. 18 (1975) 183.
[43] B.C. Allen, Tans. AIME 236 (1966) 903.
[44] E.N. Hodkin, M.G. Nicholas, D.M. Poole, J. Less-Common Met. 20 (1970) 93.
[45] S.V. Radcliffe, J. Less-Common Met. 3 (1961) 360.
[46] H. Mykura, Acta Metall. 3 (1955) 436.
[47] A.R. Miedema, F.J.A. den Broeder, Z. Metallkd. 70 (1979) 14.
[48] J. Xu, J.S. Yin, E. Ma, Nanostruct. Mater. 8 (1997) 91.
[49] J. Eckert, J.C. Holzer, C.E. Krill III, W.L. Johnson, J. Mater. Res. 7 (1992) 1751.
[50] H.J. Fecht, E. Hellstern, Z. Fu, W.L. Johnson, Metall. Trans. A 21 (1990) 2333.
[51] Y.H. Zhao, K. Lu, K. Zhang, Phys. Rev. B 66 (2002) 085404.
[52] Y.H. Zhao, H.W. Sheng, K. Lu, Acta Mater. 49 (2001) 365.
[53] I. Lucks, P. Lamparter, E.J. Mittemeijer, Acta Mater. 49 (2001) 2419.
[54] J. Xu, J.H. He, E. Ma, Metall. Trans. A 28 (1997) 1569.

[55] Z. Chen, G.R. MacKay, D.A. Small, R.A. Dunlap, J. Phys. D: Appl. Phys. 32 (1999) 1934.
[56] X. Zhang, H. Wang, J. Narayan, C.C. Koch, Acta Mater. 49 (2001) 1319.
[57] F.A. Mohamed, Acta Mater. 51 (2003) 4107.
[58] Y.H. Zhao, X.Z. Liao, Y.T. Zhu, Z. Horita, T.G. Longdon, Mater. Sci. Eng. A 410&411 (2005) 188.
[59] Y.H. Zhao, X.Z. Liao, Y.T. Zhu, Z. Horita, T.G. Longdon, Mater. Sci. Eng. A, in press.
[60] J.J. Hauser, Phys. Rev. B 17 (1978) 1908.
[61] L.B. Davis, P.J. Grundy, J. Non-Cryst. Solids 11 (1972) 179.
[62] J.R. Bosnell, Thin Solid Films 3 (1969) 233.